J Appl Electrochem (2010) 40:1779–1787
DOI 10.1007/s10800-010-0113-y

ORIGINAL PAPER

Electroxidation of oxalic acid at different electrode materials

S. Ferro · C. A. Martínez-Huitle · A. De Battisti

Received: 2 February 2010 / Accepted: 15 March 2010 / Published online: 27 March 2010

Abstract Oxalic acid is one of the proposed metabolites of the anodic oxidation of more complex organic molecules. In spite of its simple structure, its mineralization strongly depends on the nature of the electrode material at which the process is carried out. Sargisyan and Vasil'ev (Elektrokhimiya 18:845, 1982) pointed out such dependence, investigating the kinetic behavior of OA at different metal (Rh, Pd, Os, Ir, Pt and Au), at dimensionally stable anodes (RuO_2–TiO_2) and at glassy carbon (GC) electrodes. Their conclusions highlighted the important role played by the organic anion adsorption step, claiming that OA is oxidized with increasing difficulty at electrode materials having higher oxygen affinity. More recently, these assumptions have been supported by data on OA oxidation at high anodic potentials (Martínez-Huitle et al., Electrochim Acta 49:4027, 2004). To further enrich the picture, in the present paper, kinetic investigations were carried out at different mixed-oxides, Pt, GC and highly conductive, boron-doped diamond (BDD) electrodes, with either oxygen or fluorine at their surface.

Keywords Oxalic acid · Electrochemical incineration · Kinetics · Electrode material · Adsorption

S. Ferro · C. A. Martínez-Huitle · A. De Battisti (✉)
Department of Biology and Evolution, University of Ferrara,
via L. Borsari 46, 44121 Ferrara, Italy
e-mail: dbtcll@unife.it

Present Address:
C. A. Martínez-Huitle
Departamento de Química, Centro de Ciências Exatas e da Terra,
Universidade Federale do Rio Grande do Norte,
Lagoa Nova, Natal CEP 59 072-970, Brazil

1 Introduction

The anodic oxidation of oxalic acid (OA) has been extensively studied, as a model reaction, somewhat at the border between organic and inorganic electrochemistry [1–28]. The interest for this reaction is further increased because of its implication in industrially important ethylene glycol oxidation [29, 30, 31] and in the electrochemical incineration of polluting organic substrates in wastewater [32–34]. Most studies have been carried out at Pt electrodes [1–23], although other electrode materials have been taken into consideration, like Pd [24, 25], Au [25, 26], as well as conductive-oxide materials, like RuO_2–TiO_2 [1], TiO_2 [27], RuO_2 [27], WO_x [28] and IrO_2–Ta_2O_5 [32]. The wealth of experimental evidence has led to the proposal of different oxidation mechanisms, although no complete agreement has been attained on the nature of adsorbed intermediates, and details of the reaction mechanism are not completely elucidated so far. The study of the adsorption of OA at Pt electrodes [9, 10, 16, 18, 19] has shown the existence of two types of adsorbed species: the first is a strongly bound one, which completely desorbs at $E = 0.4$–0.6 V (vs. RHE), and with a CHO-type stoichiometry [6]; the second is a weakly bound, anion-like species [20].

As far as the electroxidation of OA is concerned, two mechanisms seem of particular interest (e.g. [3]). The first of them assumes an electrosorptive first step, followed by a destructive chemical-desorption-step of the adsorbed intermediate HC_2O_4:

$$H_2C_2O_4 \rightarrow HC_2O_{4(ads)} + H^+ + e \quad (1)$$

$$HC_2O_{4(ads)} \rightarrow 2CO_2 + H^+ + 2e \quad (2)$$

In the second mechanism, a first step where OA is adsorbed at the electrode surface is hypothesized, followed by the

hydroxyl radical electrosorption step and eventually by the surface reaction of the two adsorbed species [9]:

$$H_2C_2O_4 \rightarrow H_2C_2O_{4(ads)} \quad (3)$$

$$H_2O \rightarrow OH_{(ads)} + H^+ + e \quad (4)$$

$$H_2C_2O_{4(ads)} + 2OH_{(ads)} \rightarrow 2CO_2 + 2H_2O \quad (5)$$

The co-existence of substantially different mechanisms encourages further research at electrode materials with different hydrophilicity and different catalytic activity toward the oxygen evolution reaction, whose first step is the hydroxyl radical formation.

In this work, an analysis of the dependence of OA electroxidation on the nature of the electrode material was attempted at Pt, glassy carbon (GC) and different mixed-oxide, DSA-type electrodes, and subsequently extended to highly conductive, boron-doped diamond (BDD) thin films, with both oxygen and fluorine at their surfaces.

2 Experimental details

All measurements were performed with an Autolab PGSTAT20, equipped with a SCANGEN module (Ecochemie, The Netherlands), and using an electrolysis cell made of Teflon® and glass. The working electrode, set at the bottom of the cell, with only the upper surface in contact with the electrolyte solution, had a nominal area of 0.785 cm^2 (a disk with a diameter of 1 cm). The counter electrode was a cylindrical platinum grid, and potentials were measured against a double-walled, saturated calomel electrode (SCE), with an intermediate saturated $NaNO_3$ solution.

Measurements were carried out in solutions of OA (Fluka, dihydrate salt) at concentrations ranging between 0.1 and 0.75 M, using 1 M $HClO_4$ (Fluka) as the background electrolyte; $NaClO_4$ monohydrate (Fluka) was used in order to maintain a constant ionic strength. Chemicals were of analytical grade, and all solutions were prepared with MilliQ water ($\rho > 18$ MΩ cm). Initial investigations were performed by cyclic voltammetries (CV) at room temperature, and at a scan rate of 100 mV s^{-1}. The chosen potential range was cycled using a step potential of 2 mV and repeating the measurement at least five times or until reproducible signals were obtained; in each case, the last cycle was recorded. Quasi-steady polarization curves were recorded in solutions stirred by bubbling nitrogen, at a scan rate of 0.5 mV s^{-1} and with a step potential of 0.45 mV, starting from the higher value and conditioning the electrode at the initial potential for 15 s. The stability of electrode materials was tested recording a CV curve before and after every polarization. The following electrode materials were investigated: platinum, GC, Ti/IrO_2–Ta_2O_5, Ti/IrO_2–2SnO_2, Ti/$Ir_{0.67}Ru_{0.33}O_2$–2SnO_2, Ti/RuO_2–2SnO_2, and both fluorine- [35] and oxygen-terminated [36] BDD films. Both BDD and F-BDD films were kindly provided by CSEM (now Adamant Technologies, Neuchâtel, Switzerland); oxygen-termination on the BDD surface was obtained electrochemically by either cycling the electrode between hydrogen and oxygen evolution onsets (in 1 M $HClO_4$: mildly oxidized BDD), or pre-treating it at +3 V versus SCE, for 20 min (strongly oxidized BDD).

A sol–gel method was applied to synthesize the Ti-supported IrO_2–2SnO_2, $Ir_{0.67}Ru_{0.33}O_2$–2SnO_2 and RuO_2–2SnO_2 oxide coatings [37], while Ti/IrO_2–Ta_2O_5 electrodes were kindly supplied by Industrie DeNora (Milan, Italy).

3 Results and discussion

3.1 Pt and glassy carbon

Measurements at Pt and GC were carried out in order to ensure the consistency of our results with those described in the literature, and to make available a reference basis with which the results at oxide electrodes and BDD could be compared. As far as CV data are concerned, no differences with the literature were found, and thus they are not shown in this paper. In agreement with refs. [11, 14, 21–23], CV curves at the Pt electrode in the presence of OA show that the organic molecule adsorbs at the electrode surface, as witnessed by the modification of hydrogen adsorption and desorption peaks, which are shifted towards more negative potentials when OA is present in the solution. This behavior is characteristic of a weak adsorption, similar to that generally observed in the case of anions. The OA oxidation peak appears as a single signal between 0.8 and 0.9 V and, in the explored range (from 1 to 100 mM), its height depends on OA concentration [2]. In a previous paper, experiments were carried out in acidic media (0.5 M H_2SO_4) [2]; however, the catalytic activity of Pt for the OA oxidation was shown to depend on pH and nature of supporting electrolyte [11, 14]. Chollier et al. [11] found that the reaction is rather inhibited by chloride anions and is faster in the presence of ClO_4^- and HSO_4^-; in addition, the Pt electrocatalytic activity was higher in perchloric than in sulfuric acid, at a pH $\approx$0.5.

CV curves recorded at a Ti/Pt electrode are quite similar to those obtained at Pt, and corresponding results were obtained also from quasi-steady polarization curves. It is worth mentioning that other authors carried out measurements using either platinized Pt or smooth platinum electrodes, and thus considering different roughness factors: no significant mechanistic differences were found [1, 3, 4, 6, 9, 11]. In fact, at variance with that of other organic compounds, the rate of the OA oxidation reaction does not

depend on electrode roughness, possibly because of the lack of dimensional effects, not important in the case of the small OA molecule [38]. On the other hand, Petrii and coworkers [3] recorded polarization curves, in the potential range of water oxidation, pointing out the existence of a pronounced hysteresis. An inhibition of the process, caused by a preliminary polarization at oxygen-evolving potentials, has been described also by Horanyi et al. [16], on the basis of measurements in solutions containing $HClO_4$ as the supporting electrolyte. It can be assumed that the nature of the anion of the supporting electrolyte, which adsorbs together with oxygen-species and OA, may affect the ratio between components in a mixed adsorption layer. Horanyi's later experiments [18], carried out in H_2SO_4 solutions at different concentrations, proved that sulfate anions can force out the OA adsorption products. Beside this effect, adsorbed oxygen species can play an additional inhibiting role.

E/*J* plots at a pre-oxidized Pt electrode, in the presence of different concentrations of OA, are shown in Fig. 1. The electrochemical oxidation of OA seems to be strongly hindered under these conditions, and the intersection of polarization curves at about 1.8 V underlines the complex set of electrochemical reactions taking place at the oxidized Pt surfaces, involving most probably the o.e.r. as the main process [2].

CV experiments at the GC electrode (Fig. 2) showed that OA is electroactive at this material, its oxidation taking place about 300–400 mV before the o.e.r. onset. In addition, a signal centred at about 0.9 V (vs. SCE) was observed for OA concentrations ≥500 mM. The literature reports that OA oxidation takes place across a wide potential range (see, for example, ref. [1]); however, the effect is witnessed only by an increase in current density and a shift of quasi-steady polarization curves to less positive potential values, with increasing the OA concentration (Fig. 3). Tafel slopes from 110 to 121 mV decade^{-1}, and a reaction order of about 0.7, with respect to OA concentration, were obtained. A significantly higher Tafel slope (about 220 mV decade^{-1}) was previously reported by Sargisyan and Vasil'ev [1]: such a big difference may be related to changes in electrode surface state, as a result of the higher anodic potential explored in [1].

3.2 Mixed-oxide (DSA-type) electrodes

Figure 4 shows cyclic voltammograms for a Ti/IrO_2–Ta_2O_5 anode, recorded between 0.15 and 1.15 V (vs. SCE), at a potential scan rate of 100 mV s^{-1}. The addition of the organic substrate has no significant effect on the shape of CV curves, with the exception of a quite modest increase in currents in the oxygen evolution potential range ($E > 1.15$ V). This experimental evidence, coupled with indication of the lack of solid solutions between IrO_2 and Ta_2O_5, could be due to a poor catalytic activity of pure IrO_2 surfaces toward the anodic oxidation of the organic substrate. However, considering the competitive character of $OH^{\bullet}$ adsorption, the evidence in Fig. 4 could be also justified in terms of a preferential interaction between active sites and hydroxyl radicals themselves, which would result in the hindrance of OA adsorption as well. Only at higher substrate concentrations, some moderate degree of adsorption would be achieved.

As shown in Fig. 5, at variance with the above experimental evidence, OA exhibits a quite important electroactivity at the Ti/IrO_2–$2SnO_2$ electrode: the organic oxidation onset can be placed at about 0.8 V versus SCE, thus 350–400 mV prior to the beginning of the o.e.r. As data on IrO_2–Ta_2O_5 also indicate, this cannot be easily accounted for if only the role of the "active" component, IrO_2, is considered. On the other hand, as elsewhere shown [39],

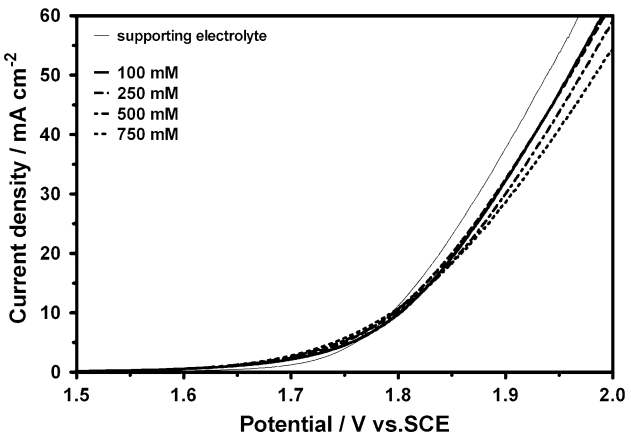

Fig. 1 Polarization curves for the electroxidation of OA at the Pt electrode

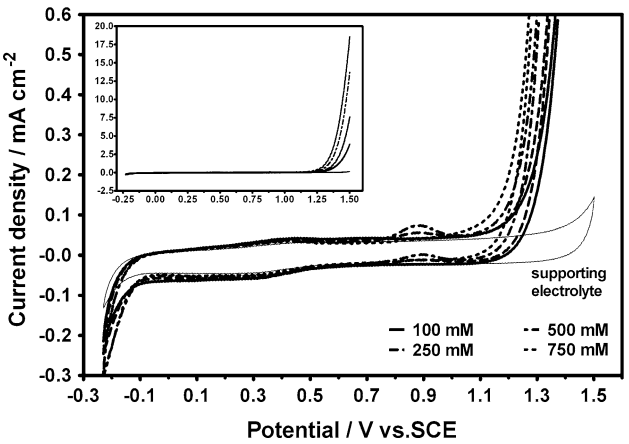

Fig. 2 Magnification of CV curves for the GC electrode, in the presence of the pure supporting electrolyte and of different amounts of OA in solution. *Inset* the whole experimental picture

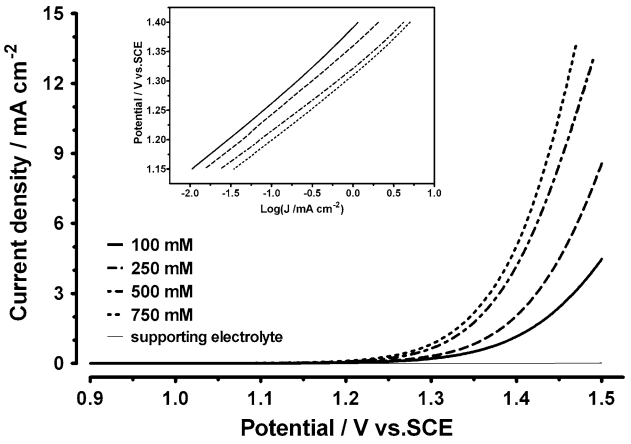

Fig. 3 Polarization curves for the GC electrode, in the presence of the pure supporting electrolyte and of different amounts of OA in solution. *Inset* elaboration of data in terms of Tafel plot

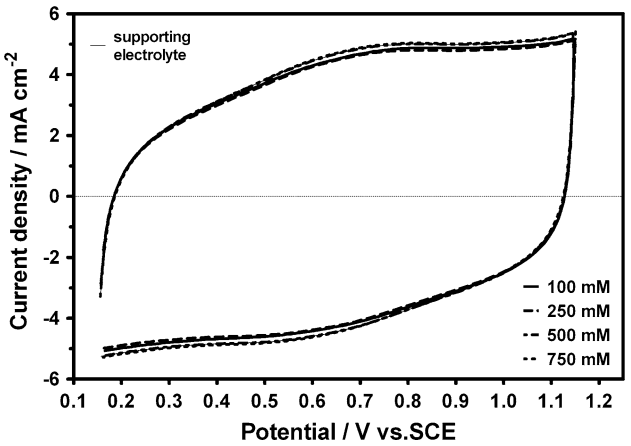

Fig. 4 CV curves for a Ti/IrO_2–Ta_2O_5 electrode, in the presence of the pure supporting electrolyte (1 M $HClO_4$) and with OA in solution; data obtained at 100 mV s^{-1}

this binary system consists of a substitutional solid solution between the two oxide components and its surface consist of Sn(IV) and Ir(IV) sites belonging to one and the same conductive substitutional solid solution. This may well have electronic effects related with the structure of the two M^{4+} ions (d^{10} Sn^{4+} and d^5 Ir^{4+}) as well as with the increase in the *a* and *c* tetragonal lattice parameter. As a matter of fact, the detail of the shape of the voltammograms for IrO_2–Ta_2O_5 and IrO_2–SnO_2 mixed-oxide electrodes is significantly different, already in pure supporting electrolyte. In the case of the Ta_2O_5-stabilized coating, a single broad and shallow maximum is observed, while the SnO_2-stabilized coating presents two partially convoluted peaks, with a quite pronounced reversibility of the charging process. Interestingly, the raise of the current related with OA oxidation begins at the foot of the second peak. On the basis of the limited information available, the second weak signal in the blank voltammogram could be assigned to the electroactivity of less easily oxidizable sites at the mixed-oxide surface. It could be assumed that OA adsorption takes place just before the latter solid-state redox process, leading to the substrate oxidation.

The electrochemical behavior of OA at a Ti/$Ir_{0.67}Ru_{0.33}O_2$–$2SnO_2$ electrode is shown in Fig. 6. The onset of OA electroxidation is located, as in the previous case, close to 0.8 V; however, the current response for one and the same substrate concentration is at least twice as much, compared with that recorded at the Ti/IrO_2–$2SnO_2$ film electrode (Fig. 5). As witnessed by the lower voltammetric currents recorded at the ternary-mixture electrode, this cannot be accounted for by a larger electrochemically active area of the coating.

The sensitivity of the reaction to the electrode composition is further confirmed by data in Fig. 7, recorded at a Ti/RuO_2–$2SnO_2$ coating. The current increase due to OA addition is still important, but the onset of its oxidation is shifted by about 100 mV in the positive direction, accompanying the foot of a poorly pronounced voltammetric peak in the blank CV. In this case, maxima would fall in the o.e.r. region. Even if not all the possible combinations of components have been taken into consideration in this work, the CV evidence underlines the decisive importance of the presence of SnO_2 as a film component, whose role is further modulated by group VIII noble-metal oxides.

To gain additional insight into these aspects, the electrochemical behavior of OA has been further investigated by quasi-steady polarization curves, and related diagnostic parameters. As shown in Fig. 8 (blank curve), at a Ti/IrO_2–Ta_2O_5 the o.e.r. is anticipated with respect to what was observed at oxidized Pt surfaces (Fig. 1). Currents due to OA oxidation remain quite low up to the oxygen evolution and the features of *J*/*E* curves are affected by the presence of OA in a fairly complex way. Current values obtained in

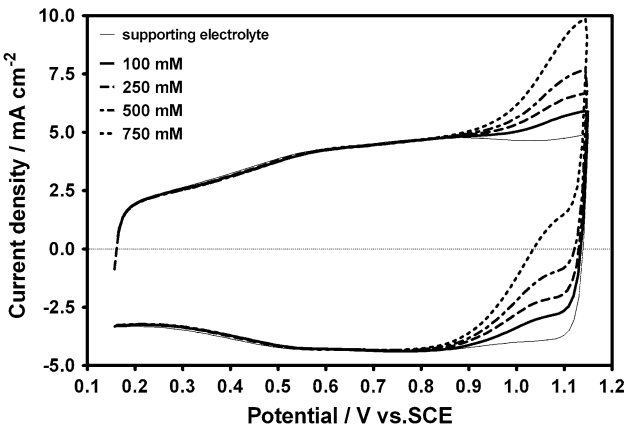

Fig. 5 CV curves for a Ti/IrO_2–$2SnO_2$ electrode, in the presence of the pure supporting electrolyte (1 M $HClO_4$) and with OA in solution; data obtained at 100 mV s^{-1}

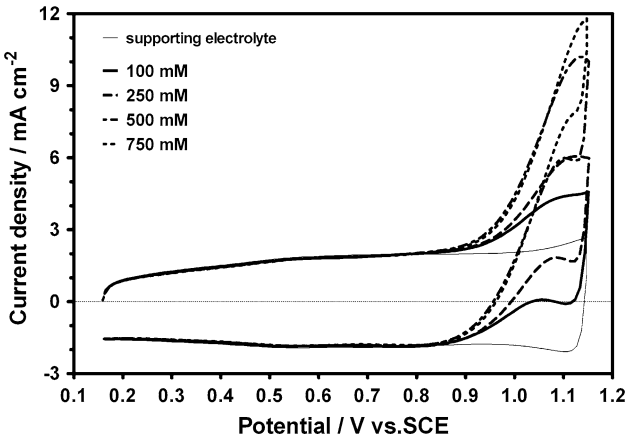

Fig. 6 CV curves for a Ti/$Ir_{0.67}Ru_{0.33}O_2$–$2SnO_2$ electrode, in the presence of the pure supporting electrolyte (1 M $HClO_4$) and with OA in solution; data obtained at 100 mV s^{-1}

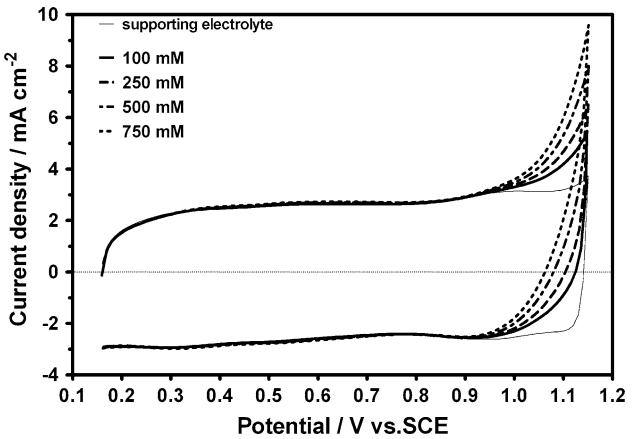

Fig. 7 CV curves for a Ti/RuO_2–$2SnO_2$ electrode, in the presence of the pure supporting electrolyte (1 M $HClO_4$) and with OA in solution; data obtained at 100 mV s^{-1}

the presence of low substrate concentrations (100–500 mM) indicate a significant inhibitive action toward the o.e.r., with no evidence of electroactivity of the organic substrate. At the highest OA concentration, 750 mM, a moderate electroactivity appears between about 1.00 and 1.25 V, where the o.e.r. is absent or occurs at a very low rate. At potentials higher than ~1.25 V, the *J/E* curves intersect the blank one, and a sort of poisoning of the catalytic activity of IrO_2 toward the o.e.r. is the main feature. Although this IrO_2-based electrode is much more active than Pt toward the o.e.r., its behavior in the presence of OA is quite similar.

Experiments were carried out also at a Ti/IrO_2–$2SnO_2$ electrode, and results are shown in Fig. 9. In agreement with the CV data of Fig. 5, the onset of the OA oxidation is located in the potential range 0.80–0.90 V, much lower with respect to the threshold of about 1.20 V at which the oxygen evolution starts. In fact, no significant contribution

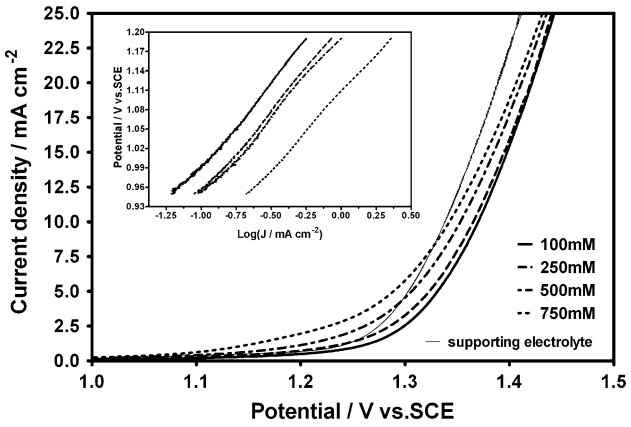

Fig. 8 Polarization curves for a Ti/IrO_2–Ta_2O_5 electrode, at different OA concentrations. *Inset* elaboration of data in terms of Tafel plot

from the solvent oxidation to the total anodic current is observed up to at least 1.30 V. An interesting feature of quasi-steady *J/E* curves in Fig. 9 is a passivation effect, resulting in the plateau between ~1.10 and 1.15 V. The reason for the drop in the oxidation rate of OA could be sought in the oxidation state changes that IrO_2 undergoes in the above relatively narrow potential window. A further increase in the potential above 1.17–1.18 V leads, however, to a recovery of the catalytic activity of the electrode surface with a consequent increase in *J*. As shown in the inset of Fig. 9, two distinct linearity regions can be found in *E*/log *J* plots, prior to the o.e.r., with essentially the same slope but different intercept. On the basis of the relevant literature, the possibility of co-existing mechanisms at Pt and Pt/Pt surfaces has been proposed, *e.g.* by Schiffrin et al. [17], and the present data at IrO_2–$2SnO_2$ electrode seem to supply further evidence to this point. A Tafel slope close to 0.12 V $decade^{-1}$, for the first linear segment in the insert, would be in agreement with the mechanism proposed by Sargisyan and Vasil'ev [1], while the substantially similar slope of the second segment could fit in a model, like that proposed by Inzelt et al. [9], where the rate determining step is rather the hydroxyl radical formation, followed by the bimolecular surface reaction between $OH^{\bullet}$ and adsorbed OA.

From Tafel plot data (inset of Fig. 9), a reaction order of about 0.75 could be estimated, revealing a strong surface activity toward OA oxidation. Tafel slopes, at the different OA concentrations (from 0.1 to 0.75 M), were 157, 120, 115 and 100 mV $decade^{-1}$, respectively.

Quasi-steady polarization curves for OA electroxidation at Ti/$Ir_{0.67}Ru_{0.33}O_2$–$2SnO_2$ are shown in Fig. 10 and they confirm, together with CV results of Fig. 6, a high reactivity of OA between 0.80 and 1.10 V. The passivation effect observed in Fig. 9 at the Ti/IrO_2–$2SnO_2$ is even more evident at the ternary mixture, and a minimum in *J* is

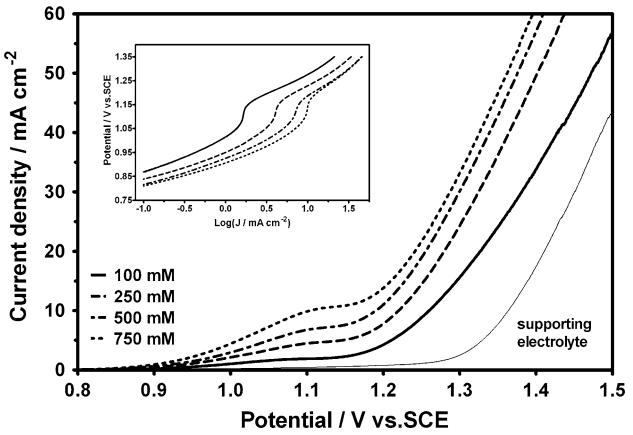

Fig. 9 Polarization curves for a Ti/IrO_2–$2SnO_2$ electrode, at different OA concentrations. *Inset* elaboration of data in terms of Tafel plot

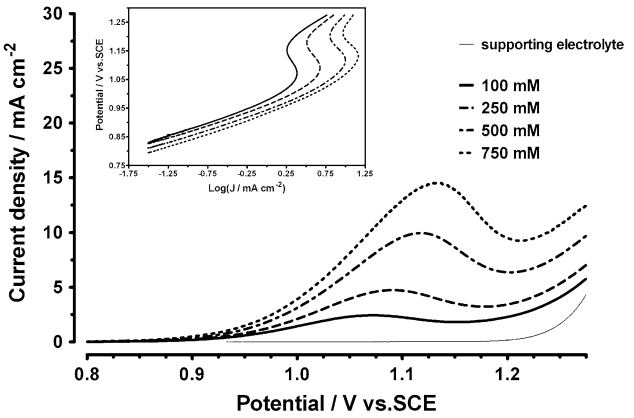

Fig. 10 Polarization curves for a Ti/$Ir_{0.67}Ru_{0.33}O_2$–$2SnO_2$ electrode, at different OA concentrations. *Inset* elaboration of data in terms of Tafel plot

observed at about 1.2 V. At higher potentials, in correspondence with the onset of the o.e.r. (in the blank solution) or slightly before it, the passivation effect disappears, but in this case the o.e.r. would be expected to contribute to the *J* and this limits the interest of the information obtained from *J*/E curves beyond roughly 1.20 V, related to a mixed process. Tafel slopes have values of about 90–95 mV decade^{-1}, independently of OA concentration (inset of Fig. 10). Under these conditions, the mechanism proposed by Bockris et al. [6] and Orts et al. [20] (Eqs. 1, 2) better fits the experimental picture. As a final example of electrochemical reactivity of OA at noble-metal oxide electrodes, polarization curves at a Ti/RuO_2–$2SnO_2$ electrode are shown in Fig. 11 (the pertaining Tafel plot is reproduced in the inset): in this case, a comparison with the pure supporting electrolyte could not be obtained (RuO_2 is not stable under o.e.r. conditions). The different catalytic properties of RuO_2 with respect to IrO_2 are reflected also in the OA electrochemical oxidation, which is slightly anticipated at IrO_2 containing coatings (Figs. 9, 10), as also shown by CV data of Fig. 7. Besides, the potential range where the process inhibition is observed is shifted to more positive potentials, and superimposes with oxygen evolution. Tafel slopes are between 190 and 230 mV decade^{-1} and the reaction order with respect to the organic substrate is around 0.7.

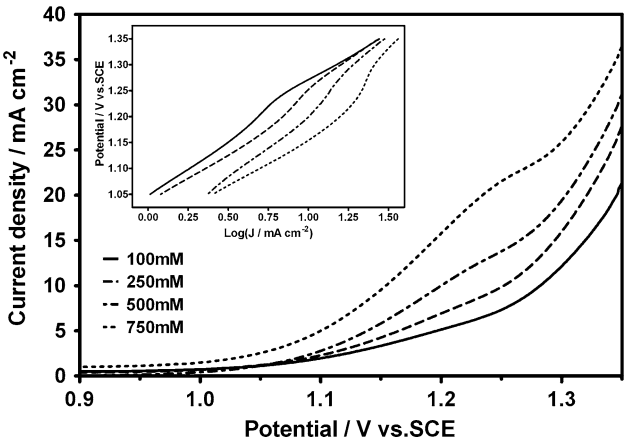

Fig. 11 Polarization curves for a Ti/RuO_2–$2SnO_2$ electrode, at different OA concentrations. *Inset* elaboration of data in terms of Tafel plot

3.3 BDD electrodes

Quasi-steady polarization experiments were carried out at fluorine-terminated BDD (F-BDD, [35]), as well as at mildly and strongly oxidized BDD surfaces [36]. Figure 12 shows polarization curves obtained at a F-BDD electrode; Tafel slopes of about 160 mV decade^{-1} were obtained (inset of Fig. 12), and the reaction order with respect to the organic reactant amounted to about 0.6. As a general feature, the oxidation of OA seems to be strongly hindered at this electrode, possibly because of the hydrophobicity of its surface and consequent poor adsorption of OA and $OH^{\bullet}$ species [35].

The electroxidation of OA was investigated, under similar conditions, at the strongly oxidized BDD. As can be seen in Fig. 13, the character of polarization curves at this electrode is similar to that discussed at the fluorinated material, with only a moderate increase in substrate electroactivity. Tafel slopes are greater than those previously discussed, ranging from 200 to 240 mV decade^{-1} (the higher value was obtained at the lowest OA concentration); also, a reaction order slightly lower than 0.55 was estimated.

Finally, the behaviour of OA at a mildly oxidized BDD electrode is shown in Fig. 14. Tafel slopes were from 170 to 215 mV decade^{-1}, and the reaction order was approximately equal to 1.2.

Different behaviours, for the different conducting diamond films, can be distinguished: OA is relatively inactive

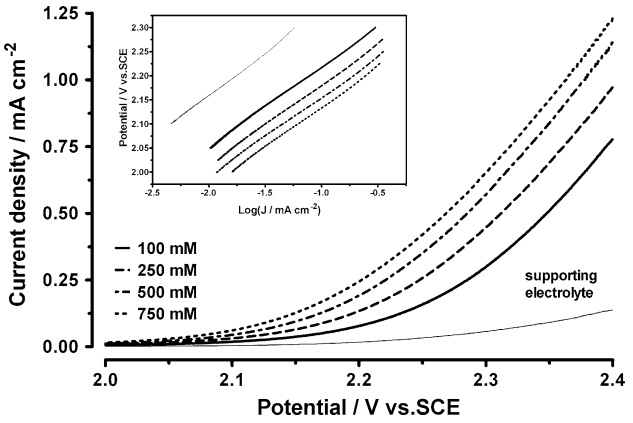

Fig. 12 Polarization curves for a F-BDD electrode, at different OA concentrations. *Inset* elaboration of data in terms of Tafel plot

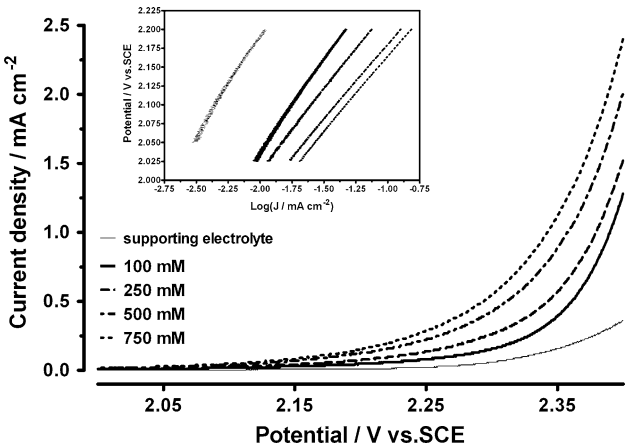

Fig. 13 Polarization curves for a strongly oxidized BDD electrode, at different OA concentrations. *Inset* elaboration of data in terms of Tafel plot

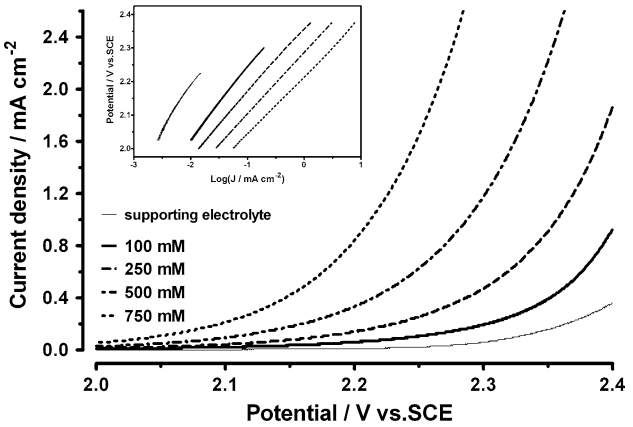

Fig. 14 Polarization curves for a mildly oxidized BDD electrode, at different OA concentrations. *Inset* elaboration of data in terms of Tafel plot

at the fluorinated electrode, while measured currents are doubled at the strongly and mildly oxidized BDD surfaces, showing a decrease in the overpotential required for the reaction. An important effect of the polarization appears to be the elimination of sp^2 species, which can be more or less abundant on the diamond surface, depending on preparation conditions. The importance of non-diamond species for electrode activity has been investigated in details by Duo et al. [40], especially in relation to electron transfer reactions: electrochemical responses varied as a function of surface treatment. Untreated electrodes (BDD as-grown or "fresh" electrodes) exhibited the highest surface activity, while the electrode response decreased significantly after anodic polarization. A relatively mild polarization process was sufficient to transform the surface from hydrophobic (BDD as-grown) to hydrophilic (BDD mildly oxidized) without changes in crystal shape and size. However, the electrochemical properties were strongly modified: for example, the voltammetric charge decreased, probably as a result of the diminution of active surface sites concentration. After stronger oxidation processes, electrodes experienced morphological changes involving both crystal size and crystal shape: the surface became smoother, and the electrochemical activity, measured in terms of voltammetric charge, decreased strongly [40]. This may explain why better results were obtained at mildly oxidized BDD, during the oxidation of OA. Moreover, based on required anode potentials, the organic oxidation clearly involves intermediates that are only available during the oxygen evolution reaction, in agreement with data obtained at BDD anodes by Comninellis et al. [12].

3.4 Mechanism discussion

Based on the literature relevant to OA and water electrooxidation, the following mechanistic hypotheses can be considered:

(a) anodic oxidation of OA:

(1) $HC_2O_4^- + M \rightarrow M\text{–}HC_2O_4^{\bullet} + e$
(2) $M\text{–}HC_2O_4^{\bullet} \rightarrow M + 2CO_2 + H^+ + e$
(3) $M\text{–}OH^{\bullet} + M\text{–}HC_2O_4^{\bullet} \rightarrow 2M + 2CO_2 + H_2O$
(4) $2M\text{–}OH^{\bullet} + HC_2O_4^- + H^+ \rightarrow M + 2CO_2 + 2H_2O$

(b) anodic oxidation of water:

(1′) $H_2O + M \rightarrow M\text{–}OH^{\bullet} + H^+ + e$
(2′) $M\text{–}OH^{\bullet} \rightarrow M\text{–}O^{\bullet} + H^+ + e$
(3′) $2M\text{–}O^{\bullet} \rightarrow 2M + O_2$

Mechanism (a) (Steps (1)–(2)) has long been proposed by several authors and requires OA electrosorption as a pre-requisite, without participation of hydroxyl radicals.

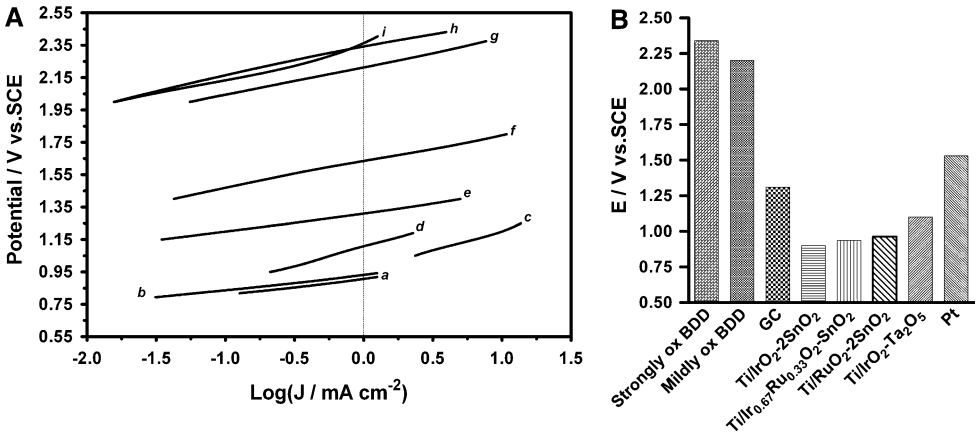

Fig. 15 **a** Tafel plot for the OA electroxidation at different electrodes; [OA] = 750 mM. (*a*) Ti/IrO_2–$2SnO_2$; (*b*) Ti/$Ir_{0.67}Ru_{0.33}O_2$–$2SnO_2$; (*c*) Ti/RuO_2–$2SnO_2$; (*d*) Ti/IrO_2–Ta_2O_5; (*e*) GC; (*f*) Pt; (*g*) mildly ox BDD; (*h*) strongly ox BDD; (*i*) F-BDD. **b** Anodic potential required to measure a current density of 1 mA cm^{-2}, at different electrodes

On the other hand, mechanism (1) + (3) implies superimposition of the organic substrate electrosorption and at least the first step of the oxygen evolution reaction. Step (4) can account for the possibility of a "direct" chemical reaction between oxidized surface of the electrode and OA in a non-adsorbed state.

Mechanistic hypothesis (b) adequately describes o.e.r. at noble-metal-oxide-based electrodes in acidic media; intermediate steps like (1′) can be represented through the general scheme:

$$MO_x(OH)_y \rightarrow MO_{x+1}OH_{y-1} + H^+ + e$$
$$(\text{with M} = \text{Ru, Rh, Pd, Os, Ir, Pt})$$

and they condition not only the catalytic activity of the oxide electrodes toward the oxygen evolution, but also their charge-storage capacity in the potential range preceding it.

The increase in potential from hydrogen evolution to oxygen evolution causes an increase in oxidation state of noble-metal-ions from (II) to (IV), higher oxidation states, i.e. (V) and (VI), being achieved at the onset of oxygen evolution itself. This could imply a progressively favored adsorption of the water molecules (hydroxyl groups), because of their smaller size and higher reorientation ability.

In order to better focus on possible interactions between noble-metal-ion sites at the electrode surface, it may be useful to refer also to data on solution equilibria involving Ir(IV), Ir(III) [41, 42], which indicate that oxalato–Ir(III) complexes are formed through a direct reaction between OA and hydrated Ir(IV). The reaction involves the Ir(IV) reduction prior to the complex formation. Electroxidation of $HC_2O_4^-$ at IrO_2–SnO_2, IrO_2–RuO_2–SnO_2, and RuO_2–SnO_2 electrodes (Figs. 5, 6, 7, 9, 10, 11) could be interpreted on the basis of the above considerations. Under potentials at which most of noble-metal sites is in the (III) form, adsorption of oxalate species may be favored and their oxidation may occur through Steps (1)–(2) in mechanism (a), prior to the oxygen evolution reaction. Further increase in electrode potential allows the attainment of higher oxidation states of the metal cations at the electrode surface, accompanied by preferential electrosorption of hydroxyl groups, displacing OA species and still too stable to act as oxidation mediators themselves. This may well lead to the inhibition of OA oxidation in a more or less limited potential range in the vicinity of the o.e.r. onset, first, and then to a change of mechanism to the (1) + (3), mechanism (a), sustained by the higher reactivity attained by hydroxyl radicals. Reaction (4) cannot be ruled out either. Details of the effect are decided by the nature of the properties of the electrode surface.

The case of the Ta_2O_5-stabilized electrode seems to be an exception with respect to SnO_2-stabilized noble-metal oxides. The reason for this may be the well documented surface segregation of the valve-metal-oxide at the electrode film surface, which could negatively affect the interaction between the substrate and electrode catalytic sites. However, at the level of the present investigation, no conclusive interpretation of the differences could be attempted avoiding the risk of speculation. Further research is necessary to give a satisfactory interpretation. The whole outcome of this work is summarized in Fig. 15, for a 0.75 M OA concentration: the electrocatalytic activity toward OA electroxidation is higher at DSA than at BDD electrodes; in addition, Pt and GC appear in an intermediate position, between the DSA and BDD systems.

From results in Fig. 15a, the potential values required to ensure a current density of 1 mA cm^{-2} at the different electrodes were calculated and results are shown in Fig. 15b (in the case of Ti/IrO_2–$2SnO_2$, an extrapolation was made, assuming a linearity of the Tafel curve down to the required potential). Somewhat expectedly, higher potential values are found for surfaces with poor adsorptive properties, like those of doped diamond in their different modifications. The case of oxidized Pt surfaces remains at intermediate levels, possibly because of the limited attitude to adsorb OA and hydroxyl radicals.

4 Conclusions

Oxalic acid is a well known reducing agent:

$$2CO_{2(g)} + 2H^+ + 2e^- \rightarrow H_2C_2O_{4(aq)}$$
$$E^\circ = -0.42 \text{ vs. SHE}$$

Despite its relatively simple molecular structure, the kinetics of its oxidation exhibit high activation energies: for instance, an E_a value of 31 kJ mol^{-1} was measured at colloidal MnO_2 surfaces [43].

The work of Sargisyan and Vasil'ev shows that the electrode surface strongly influences the kinetics of OA anodic oxidation. The present paper supports this hypothesis with data obtained at oxide electrodes, which suggest that the adsorption at stabilized RuO_2- and IrO_2-based electrodes accelerates oxidation kinetics, unless segregation of inert oxide species de-activates the surface itself (as in the case of the IrO_2–Ta_2O_5 electrode). The inevitable differences in effective surface area among the studied electrodes prevents a more rigorous interpretation of their catalytic activity, yet the obtained CV and *J*/*E* results support the view that the interaction of OA with Ru(III)–Ru(IV) and Ir(III)–Ir(IV) surface sites allows for a faster oxidation. Extension of the present research to cases where the nature of active sites is changed, keeping surface roughness constant, would allow a better understanding of this interesting kinetic behaviour.

References

1. Sargisyan SA, Vasil'ev YuB (1982) Elektrokhimiya 18:845
2. Martínez-Huitle CA, Ferro S, De Battisti A (2004) Electrochim Acta 49:4027
3. Smirnova NV, Tsirlina GA, Pron'kin SN, Petrii OA (1999) Russ J Electrochem 35:113
4. Giner J (1961) Electrochim Acta 4:42
5. El Wakkad SES, Khalafalla SE, Shams El Din AM (1958) Egypt J Chem 1:23
6. Johnson JW, Wroblowa H, Bockris JO'M (1964) Electrochim Acta 9:639
7. Johnson JW, Mueller SC, James WJ (1971) Trans Faraday Soc 67:2167
8. Horanyi G (1974) J Electroanal Chem 51:163
9. Inzelt G, Szetey E (1981) Acta Chim Acad Sci Hung 3:269
10. YuB Vasil'ev, Sargisyan SA (1986) Electrochim Acta 31:645
11. Chollier-Brym MJ, Epron F, Lamy-Pitara E, Barbier J (1999) Catal Today 48:291
12. Gandini D, Mahé E, Michaud P-A, Haenni W, Perret A, Comninellis Ch (2000) J Appl Electrochem 30:1345
13. Sargisyan SA, Vasil'ev YuB (1982) Elektrokhimiya 18:954
14. Chollier-Brym MJ, Epron F, Lamy-Pitara E, Barbier J (1999) J Electroanal Chem 474:147
15. Sargisyan SA, Vasil'ev YuB (1982) Elektrokhimiya 18:961
16. Horanyi G, Hegedüs D, Rizmayer EM (1972) J Electroanal Chem 40:393
17. Pron'kin SN, Petrii OA, Tsirlina GA, Schiffrin DJ (2000) J Electroanal Chem 480:112
18. Horanyi G, Vertes G, Hegedüs D (1973) Acta Chim Hung 79:301
19. Smirnova NV, Petrii OA, Grzejdziak A (1988) J Electroanal Chem 251:73
20. Orts JM, Feliu JM, Aldaz A, Clavilier J, Rodes A (1990) J Electroanal Chem 281:73
21. Orts JM, Feliu JM, Aldaz A, Clavilier J, Rodes A (1990) J Electroanal Chem 281:199
22. Horanyi G (1980) Electrochim Acta 25:43
23. Horanyi G, Rizmayer EM, Inzelt G (1978) J Electroanal Chem 93:183
24. Casella IG (1999) Electrochim Acta 44:3353
25. Morozova NB, Shcheblykina GE, Vvedenskii AV (1999) Russ J Electrochem 35:310
26. Albalat R, Gomez E, Sarret M, Valles E (1989) Monatsh Chem 120:651
27. Alaune Z, Mazeikiene R (1987) Liet TSR Mokslu Akad Darb Ser B 2:11
28. Bock C, Smith A, MacDougall B (2002) Electrochim Acta 48:57
29. Obmornov EV, Karetnik VG, Koptelov VI, Dosovitskaya NA, Koptelova ZP, Masalova GP, Dosovitskii EI, Ostrovskaya VN (1967) GB Patent 1,095,100; (1970) US Patent 3,531,520
30. Obmornov EV, Karetnik VG, Koptelov VI, Dosovitskaya NA, Koptelova ZP, Masalova GP, Dosovitskii EI, Ostrovskaya VN (1970) US Patent 3,531,520
31. Pogodin VA, Kaverin NI, Krutova VP, Brazhnikov VA (1993) SU Patent 1,806,127
32. Stucki S, Koetz R, Carcer B, Suter W (1991) J Appl Electrochem 21:99
33. Scialdone O, Randazzo S, Galia A, Filardo G (2009) Electrochim Acta 54:1210
34. Martinez-Huitle CA, Ferro S (2006) Chem Soc Rev 35:1324
35. Ferro S, De Battisti A (2003) J Phys Chem B 107:7567
36. Ferro S, Dal Colle M, De Battisti A (2005) Carbon 43:1191
37. Morozov A, Ferro S, Martelli GN, De Battisti A (2005) WO 2005/014885, A1
38. Konoshita K (1982) In: Conway BE, Bockris JO'M, White RE (eds) Modern aspects of electrochemistry, vol 14. Plenum Press, New York, p 557
39. Murakami Y, Ohkawauchi H, Ito M, Yahikozawa K, Takasu Y (1994) Electrochim Acta 39:2551
40. Duo I, Fujishima A, Ch Comninellis (2003) Electrochem Comm 5:695
41. Gialdini C (1910) Gaz Chim Ital 38:485
42. Kruszyna HG, Bodek I, Libby LK, Milburn RM (1974) Inorg Chem 13:434
43. Kabir-ud-Din, Fatma W, Khan Z (2004) Colloids Surf A 234:159